

Constrained multi-objective optimization of process design parameters in settings with scarce data: an application to adhesive bonding

Alejandro Morales-Hernández^{a,b,c,*}, Sebastian Rojas Gonzalez^{a,b,c,e}, Inneke Van Nieuwenhuyse^{a,b,c}, Jeroen Jordens^d, Maarten Witters^d, Bart Van Doninck^d

^a*Core Lab VCCM, Flanders Make*

^b*Research Group Logistics, Hasselt University, Agoralaan Gebouw D, Diepenbeek, 3590, Limburg, Belgium*

^c*Data Science Institute, Hasselt University, Agoralaan Gebouw D, Diepenbeek, 3590, Limburg, Belgium*

^d*ProductionS, Flanders Make, Oude Diestersebaan 133, Lommel, 3920, Limburg, Belgium*

^e*Surrogate Modeling Lab, Ghent University, Sint-Pietersnieuwstraat 33, Ghent, 9000, East Flanders, Belgium*

*Corresponding author

Email address: alejandromoraleshernandez@uhasselt.be (Alejandro Morales-Hernández)

Abstract

Adhesive joints are increasingly used in industry for a wide variety of applications because of their favorable characteristics such as high strength-to-weight ratio, design flexibility, limited stress concentrations, planar force transfer, good damage tolerance and fatigue resistance. Finding the optimal process parameters for an adhesive bonding process is challenging: the optimization is inherently multi-objective (aiming to maximize break strength while minimizing cost) and constrained (the process should not result in any visual damage to the materials, and stress tests should not result in failures that are adhesion-related). Real life physical experiments in the lab are expensive to perform; traditional evolutionary approaches (such as genetic algorithms) are then ill-suited to solve the problem, due to the prohibitive amount of experiments required for evaluation. In this research, we successfully applied specific machine learning techniques (Gaussian Process Regression and Logistic Regression) to emulate the objective and constraint functions based on a *limited* amount of experimental data. The techniques are embedded in a Bayesian optimization algorithm, which succeeds in detecting Pareto-optimal process settings in a highly efficient way (i.e., requiring a limited number of extra experiments).

Keywords: Bayesian optimization, multi-objective optimization, constrained optimization, machine learning

1. Introduction

Adhesive bonding is the engineering process of joining two surfaces together by a non-metallic substance [3]. This process occurs frequently in many engineering design contexts, such as the automotive industry [6], electronics [26] and aeronautics [10]. It is a complex process, in which several physical and chemical processes occur simultaneously [36, 32], with outcomes that are influenced by many factors (e.g., environmental conditions, material specifications, and specific process settings). Process optimization is therefore traditionally performed by experts, based on acquired knowledge and extensive experimental campaigns [5, 16]. Yet, even for experts, optimizing adhesive bonding parameters is a daunting task, due to the complex (and, essentially, black box) relationships between the process parameters, and the case specific nature of the bonding process. As a consequence, physical experiments are required in reality to detect the optimal settings for each specific case. These tend to be costly in terms of time (time to prepare the parts to be joined, time to prepare the adhesive, to join both materials and to allow the adhesive to gain its final strength) and in terms of manual labor. Moreover, data from one industrial bonding process cannot be used to optimize another process, as not only materials and adhesives may differ but also production process specifications. As a result, optimization of an adhesive bonding process is challenging and costly, even with expert knowledge available. Moreover, the experimental approach may easily yield suboptimal results with respect to other relevant performance metrics, such as production costs.

As observed in [7] (Table 2 and sections 3.1.3 and 3.2.3), evolutionary approaches (in particular, genetic algorithms) are currently the most common data science technique in engineering design optimization. This also holds for *multi-objective* engineering problems (a.o., bonding problems). Evolutionary multi-objective algorithms are applicable to black-box optimization problems, and have proven to be effective derivative-free optimizers [42]. The *Non-dominated Sorting Genetic Algorithm (NSGA-II)* [11], in particular, has been widely used in industrial process cases. Corbett et al. [9], for instance, used NSGA-II in combination with a Gaussian Process surrogate model to simultaneously optimize two objectives (force sustained by the joint and area beneath the load-displacement curve) for a novel concept for joining materials. Labbé and Drouet [23] studied designs for optimal bonding of TSL (tubular single-lap) joints using NSGA-II, highlighting the conflicting nature of mass-related and stress-related objectives. Some of the most widely used algorithms for solving *constrained* multi-objective problems are the Constrained Non-dominated Sorting Genetic Algorithm II (NSGA-II) [11, 4], the Constrained Multi-Objective Evolutionary Algorithm based on Decomposition (C-MOEA/D) [20], the Two-Archive Evolutionary Algorithm for Constrained multi-objective optimization (C-TAEA)[24] and

the Constrained Particle Swarm Optimization algorithm for Multi-Objective problems (C-MOPSO) [14]. These differ in the way in which they handle constraints: while the first three algorithms handle the constraints during the nondominated sort, the latter use adopt a penalization function approach. We refer the reader to the original publications for further details about the implementation of these algorithms.

The authors in [7] correctly warn that the focus on evolutionary algorithms may lead to a fixation effect (Challenge 3, p.9). Indeed, not all engineering design problems lend themselves to this type of analysis. Evolutionary approaches require many function evaluations, which make them ill-suited for optimizing design problems that require *expensive* (often experimental) data (in terms of time or costs involved). Even when an emulator or surrogate model (such as a neural network) is used to mitigate this issue, the search process in this type of algorithms remains largely random, with convergence speeds that are sensitive to the choice of user-defined (and often problem-specific) parameters. Moreover, most machine learning techniques that might be used as emulator (including neural networks) require lots of data to be trained, which again causes a problem when function evaluations are expensive. Finally, for problems that exhibit noise, evolutionary algorithms may require a potentially large number of replicates in order to obtain accurate estimators for the expected values of the outcomes involved; limiting the number of replicates may result in erroneous values, which may mislead the search.

In this article, we illustrate the power of a Bayesian optimization approach for the multi-objective optimization of a novel adhesive bonding process. The approach builds on the work of [34], which we adapt to a constrained setting. The main contributions of this approach include:

- The use of a Gaussian Process Regression (GPR) surrogate that explicitly accounts for the *heterogeneous noise* that is typically present in the outcomes (objective function and constraints) of the experiments [13]. Indeed, outcomes typically cannot be observed with perfect accuracy, and the magnitude of the noise may vary between different configurations. This issue is commonly overlooked in engineering optimization problems, by simply assuming that noise is non-existent (or, at best, homogeneous).
- The use of an *infill criterion* or *acquisition function* to sequentially (one-by-one) select new process parameter configurations to be evaluated. This acquisition function balances exploration and exploitation in the search for the optimal solutions, using information from the GPR model and a Logistic Regression classification model (to predict the feasibility of bonding process configurations). It provides an explainable approach, as opposed to the upfront parameter choices that

guide the generation of successive populations in evolutionary algorithms.

- Results show that the approach is able to obtain *better* configurations than evolutionary algorithms (w.r.t. average hypervolume), while drastically reducing the number of expensive evaluations required. The approach is particularly meant for settings where the analyst can only afford a very limited number of observations; as it is general, it may constitute a powerful tool also in other data-constrained engineering design settings.

The remainder of this article is organized as follows. Section 2 discusses the main concepts in multi-objective optimization, while Section 3 describes the bonding process problem under study. Section 4 details the main concepts of Bayesian optimization, and the proposed algorithm. Section 5 discusses the design of experiments, while Section 6 compares the results with those of competing evolutionary algorithms (constrained NSGA-II, C-MOEA/D, C-TAEA, C-MOPSO). Section 7 summarizes the findings and highlights some future research directions.

2. Multi-objective optimization

In general, a multi-objective optimization problem can be defined as (assuming minimization of all the objectives):

$$\begin{aligned}
 \min \quad & [f_1(\mathbf{x}), \dots, f_m(\mathbf{x})] \\
 \text{s.t.} \quad & g_i(\mathbf{x}) \leq 0, i = 1, 2, \dots, q, \\
 & h_j(\mathbf{x}) = 0, j = 1, 2, \dots, p
 \end{aligned} \tag{1}$$

where $\mathbf{x} = [x_1, \dots, x_d]^T$ is a vector of d decision variables in the decision space D , $f : D \rightarrow \mathbb{R}^m$ is a vector-valued function yielding the m objectives, and the functions g_i ($i = 1 \dots p$) and h_j ($j = 1 \dots q$) define inequality and equality constraints, respectively. The goal of a multi-objective problem is to find the set of *non-dominated* or *Pareto-optimal* solutions. A solution $\mathbf{x}^{(1)}$ is said to dominate another solution $\mathbf{x}^{(2)}$ when it performs better than the latter on at least one objective, while not performing worse on any of the other objectives [30]. More formally, for $\mathbf{x}^{(1)}$ and $\mathbf{x}^{(2)}$ two vectors in D :

- $\mathbf{x}^{(1)} \prec \mathbf{x}^{(2)}$ means $\mathbf{x}^{(1)}$ dominates $\mathbf{x}^{(2)}$ iff $f_j(\mathbf{x}^{(1)}) \leq f_j(\mathbf{x}^{(2)}), \forall j \in \{1, \dots, m\}$, and $\exists j \in \{1, \dots, m\}$ such that $f_j(\mathbf{x}^{(1)}) < f_j(\mathbf{x}^{(2)})$
- $\mathbf{x}^{(1)} \prec\prec \mathbf{x}^{(2)}$ means $\mathbf{x}^{(1)}$ strictly dominates $\mathbf{x}^{(2)}$ iff $f_j(\mathbf{x}^{(1)}) < f_j(\mathbf{x}^{(2)}), \forall j \in \{1, \dots, m\}$

The optimizers of the individual objectives are not usually of particular interest for the decision-maker, since these only reflect the extremes of the so-called *Pareto front* (i.e., the evaluation of the Pareto set in the objective space). The geometry of the Pareto front can be very diverse (see, e.g., Figure 1 for two examples generated from artificial test problems), and is usually unknown upfront.

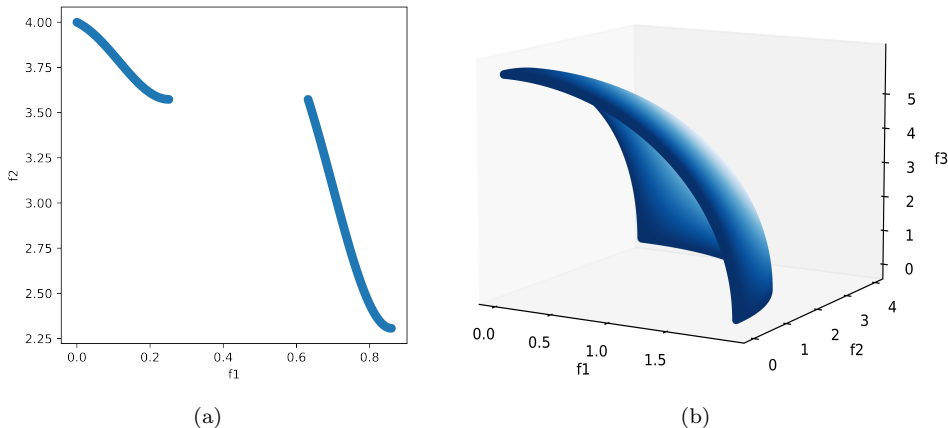


Figure 1: Illustration of (a) a 2-objective problem with a disconnected Pareto front, (b) a 3-objective problem with a concave Pareto front

The reader is referred to [29] for a comprehensive survey on *deterministic* multi-objective methods for engineering problems; in such methods, it is assumed that the objective (and, potentially, constraint) functions can be observed without noise (e.g., through a deterministic simulator, or noise-free experiments). In practice, however, the objective and constraint observations are often *noisy* [13]. The literature on *stochastic* multi-objective optimization algorithms is scarce, and consists mainly of evolutionary algorithms (see e.g., [8]), and Bayesian multi-objective optimization algorithms (see e.g., [35]).

3. Adhesive bonding process problem

The bonding process we focus on joins two PolyPhenylene Sulfide (PPS) substrates using Araldite 2011 adhesive. Figure 2 shows the general procedure of the adhesive bonding process.

The optimization focuses on the Plasma treatment step. The plasma treatment chemically modifies the top surface layer of the PPS substrate so that the surface energy increases, which impacts the adhesion strength (i.e., the strength of the connection between the adhesive and the substrate). In this process, six parameters play a role: (1) whether the surface is pre-processed or not (cleaning to remove dust and grease, which may prevent a good connection between the adhesive and the substrate), (2) the power



Figure 2: Schematic overview of the adhesive bonding process

setting of the plasma torch, (3) the speed at which the plasma torch moves across the samples, (4) the distance between the plasma torch nozzle and the sample, (5) the number of passes of the plasma torch over the sample, and (6) the time between the plasma treatment and the application of the glue (as the plasma effect reverses over time). The adhesion strength is very sensitive to the configuration of these parameters.

Using lab experiments, stress tests can be performed to check the outcomes of samples that have been treated with any particular plasma parameter configuration: the lap shear strength of the sample (MPa), the failure mode (adhesive, cohesive or substrate failure), the production cost of the sample (in euros), and the potential occurrence of visual damage (the substrates will burn when heated above their maximum allowable temperature during plasma treatment). Such physical experiments are expensive, as they require the whole process in Figure 2 to be performed, involving a human operator. Figure 3 shows an illustration of different failure modes, and an example of visual damage.

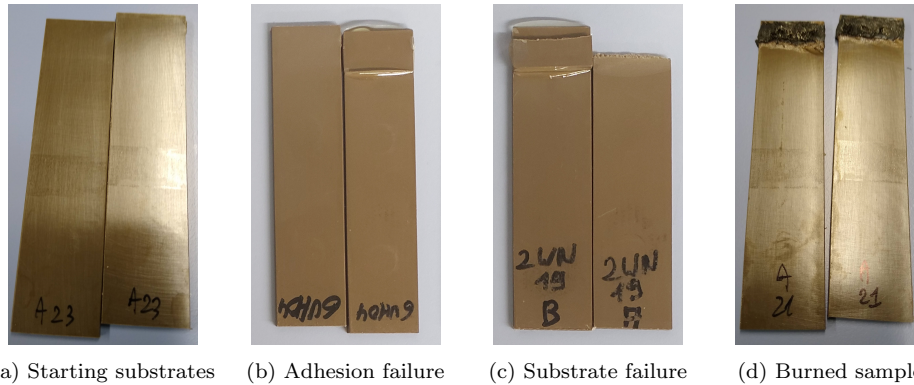


Figure 3: Illustration of failure modes that may result from the stress test applied to a sample. The adhesive is applied on the substrates (a) and the failure mode can be either adhesion failure (b), substrate failure (c) or cohesive failure (not shown). In addition, visual damage might be observed after the experiment; e.g., burned sample (d)

The goal of the optimization is to set the plasma process parameters in such a way that (1) the tensile strength (TS) is maximized, while (2) production cost (PC) is minimized, and (3) adhesive failures and visual damage are

avoided. As the objectives (1) and (2) are in conflict, this is a *multi-objective* optimization problem: the goal is to find a set of solutions that reveal the essential trade-offs between these objectives (i.e., those solutions for which no objective can be improved without negatively affecting the performance of any other objective), while meeting the constraints (3). Eq. 2 formally defines this optimization problem:

$$\begin{aligned} \min \quad & [-TS(\mathbf{x}), PC(\mathbf{x})] \\ \text{s.t.} \quad & 0.5 - Pf(\mathbf{x}) \leq 0 \end{aligned} \tag{2}$$

where the notation $Pf(x)$ refers to the probability that a process configuration x is feasible (estimated as the fraction of replications in which the configuration resulted in a feasible outcome).

As the performance evaluation is expensive, the optimization algorithm should be able to detect (nearly) Pareto-optimal solutions within a small number of experiments required; we just cannot afford to collect large amounts of experimental data. In the following section, we discuss how the use of Gaussian Process Regression combined with Bayesian optimization allows us to develop such a data-efficient optimization approach.

4. Bayesian optimization: main concepts and proposed algorithm

In this section, we first discuss the main concepts of Bayesian optimization. Next, we discuss the details of the proposed constrained multi-objective optimization algorithm (referred to as MO-GP).

4.1. Bayesian optimization: main concepts

Bayesian optimization is a supervised learning technique that builds a probabilistic metamodel, usually a Gaussian process regressor (also referred to as a *kriging model* [21, 38, 13]), based on all previous evaluations. Gaussian processes are not only able to predict the outcomes at unobserved solutions, but can also approximate the uncertainty around these predictions. This information is then used to decide which solution to evaluate next (also referred to as *infill point*), explicitly trading off exploration (high uncertainty) and exploitation (high quality). This trade-off is modeled by the acquisition function which quantifies how ‘interesting’ a solution is to evaluate.

The optimization procedure usually starts with the evaluation of an initial set of points with good space filling properties (e.g., latin hypercube sampling or quasi-random sequences).

More formally, the prediction of the target function at an unobserved point $\mathbf{x}^{(*)}$ is obtained through the conditional probability $P(f(\mathbf{x}^{(*)})|\mathbf{X}, \mathbf{Y})$ that represents how likely the response $f(\mathbf{x}^{(*)})$ is, given that we observed the target function at n input locations $\mathbf{x}^{(i)}, i = \{1, \dots, n\}$ (contained in

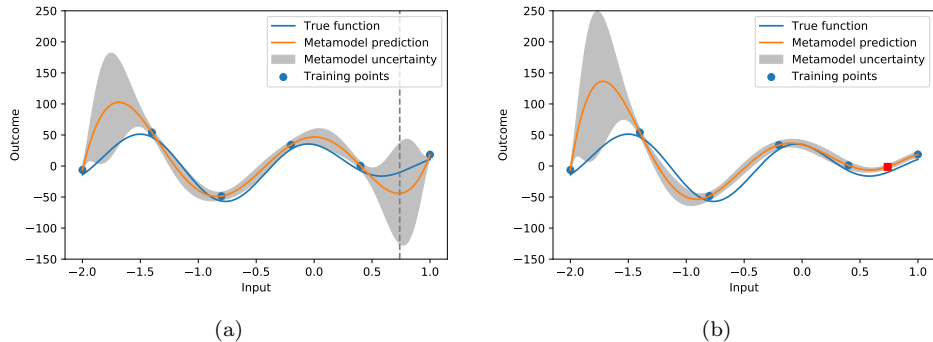


Figure 4: Selection of infill points in Bayesian optimization. At a given iteration, the solution that maximizes the acquisition function is shown as a vertical dotted line in (a). After sampling that point, the metamodel is updated including the new information (red point on (b))

matrix \mathbf{X}), yielding function values $\mathbf{y}^{(i)}, i = \{1, \dots, n\}$ (contained in matrix \mathbf{Y}). In GPR, the key assumption is that the unknown response function $y(\mathbf{x})$ follows a Gaussian process, such that

$$y(\mathbf{x}) = m(\mathbf{x}) + M(\mathbf{x}) \quad (3)$$

where $m(\mathbf{x})$ represents the mean of the process, and $M(\mathbf{x})$ is a realization of a Gaussian random field with mean zero (also referred to as the *extrinsic uncertainty* [1]). Popular choices for $m(\mathbf{x})$ are $\sum_h \beta_h f_h(\mathbf{x})$, where the $f_h(\mathbf{x})$ are known linear or nonlinear functions of \mathbf{x} , and the β_h are unknown coefficients to be estimated; β_0 , an unknown constant; or $m(\mathbf{x}) = 0$. $M(\mathbf{x})$ can be seen as a function, randomly sampled from a space of functions that, by assumption, exhibit spatial correlation according to a covariance function (also referred to as *kernel*) $k(\cdot)$:

$$\text{Cov}(\mathbf{y}^{(i)}, \mathbf{y}^{(j)}) = k(\mathbf{x}^{(i)}, \mathbf{x}^{(j)}) \quad (4)$$

Often, this covariance function is assumed to be stationary, meaning that its outcome only depends on the *distance* between the input locations. There exist multiple kernel functions in the literature [38]; in this work we use the *squared exponential* or Gaussian kernel:

$$k(\mathbf{x}^{(i)}, \mathbf{x}^{(j)}) = \sigma^2 \exp\left[-\sum_{k=1}^d (\theta_k |\mathbf{x}_k^{(i)} - \mathbf{x}_k^{(j)}|)^2\right] \quad (5)$$

where θ^2 is the process variance, and l_k is the length scale of the process along dimension k . These parameters are estimated from the already observed data, usually by means of maximum likelihood estimation.

Note that the extrinsic uncertainty in Eq. (3) is imposed on the problem by assumption, to aid the construction of the predictive model; it does not

account for the intrinsic uncertainty (i.e., the noise on the outcomes, which stems from the experiments). In our problem setting, replications of the same input location $\mathbf{x}^{(i)}$ may yield a different output $\mathbf{y}^{(r,i)}$ at each replication r . In the literature, the model in Eq. (3) is then often applied to the mean of these replications (see e.g., [13, 8, 25]). In that way, though, the analyst is neglecting the stochastic nature of the experiment, which may lead to overconfident predictions [17, 18]. To avoid this, we rely on the seminal work of [1], which provides a GP model (referred to as *stochastic kriging*) that takes into account the heterogeneous (also referred to as heteroscedastic) noise observed in the data, and models the observed response values in the r -th replication at design point $\mathbf{x}^{(i)}$ as:

$$y_r(\mathbf{x}^{(i)}) = m(\mathbf{x}^{(i)}) + M(\mathbf{x}^{(i)}) + \epsilon_r(\mathbf{x}^{(i)}) \quad (6)$$

where m and M are defined as in Eq. 3, and $\epsilon_r(\mathbf{x}^{(i)})$ is the intrinsic noise observed in replication r . The stochastic kriging prediction at an unobserved location $\mathbf{x}^{(*)}$ is then given by [1]:

$$\hat{f}(\mathbf{x}^{(*)}) = k_*[K_n + \Sigma_\epsilon]^{-1}\mathbf{Y} \quad (7)$$

with

$$K_n = [k(\mathbf{x}^{(i)}, \mathbf{x}^{(j)})], \quad i, j \in \{1, \dots, n\} \quad (8)$$

$$k_* = [k(\mathbf{x}^{(*)}, \mathbf{x}^{(i)})], \quad i \in \{1, \dots, n\} \quad (9)$$

$$\Sigma_\epsilon = \text{Diag}\left\{\frac{\text{Var}(f(\mathbf{x}^{(1)}))}{r_1}, \dots, \frac{\text{Var}(f(\mathbf{x}^{(n)}))}{r_n}\right\} \quad (10)$$

where the diagonal matrix Σ_ϵ contains the noise on the mean outcome of each already observed configuration $\mathbf{x}^{(i)}$, when this configuration has been sampled with r_i replications ($i = 1, \dots, n$).

4.2. Proposed optimization algorithm: MO-GP

Figure 5 describes the steps in the proposed constrained Bayesian multi-objective optimization approach.

The algorithm starts by evaluating an initial set of points through a Latin hypercube sample (Step 1); simulation replications are used to estimate the objective values at these points (Step 2). In the Bayesian optimization literature, it is common to set the number of initial design points equal to $k = 10d$ (with d the number of dimensions of the input space; see [28]), though also smaller design sizes have been advocated [37]. In Step 3, the augmented Tchebycheff scalarization function [22, 34] is used to transform the problem into a single-objective problem, using these training data. This approach is

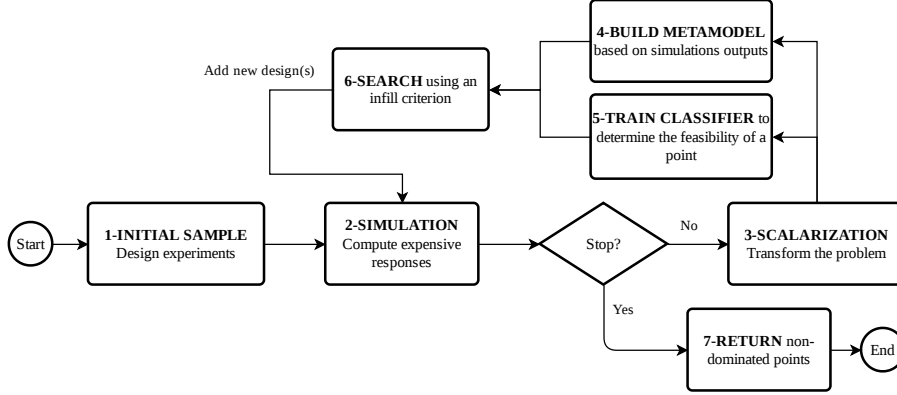


Figure 5: Proposed MO-GP approach

often used to solve general multi-objective optimization problems [31]; the scalarized objective is then given by:

$$Z_{\lambda}(\mathbf{x}) = \max_{j=\{1,\dots,m\}} \lambda_j f_j(\mathbf{x}) + \rho \sum_{j=1}^m \lambda_j f_j(\mathbf{x}) \quad (11)$$

where $\lambda = [\lambda_1, \dots, \lambda_m]$, $\sum_{j=1}^m \lambda_j = 1$, $\forall j \in \{1, \dots, m\}$, and ρ is a small positive value (e.g., $\rho = 0.05$).

We then train a (single) stochastic kriging metamodel on these scalarized objective function outcomes (Step 4); the replication outcomes are used to compute the variance of this scalarized objective. Simultaneously, a Logistic Regression (LR) classification model [40] is trained (Step 5) to predict the probability that a parameter configuration is feasible (meaning that it will not entail visual damage or adhesive failure). The LR model for d independent variables can be written as

$$P(y = 1|x, \beta) = \frac{1}{1 + e^{-(\beta_0 + \sum_{i=1}^d \beta_i x_i)}} \quad (12)$$

where $P(y = 1)$ is the probability that the outcome is feasible, and β_0, \dots, β_d are regression coefficients. Maximum likelihood estimation is used to obtain the optimal parameter values β . The LR classifier is trained using the most common output observed over the replications of a given input configuration (binary class output, with 1 if the configuration is feasible and 0 otherwise).

The information from the stochastic kriging model allows the analyst to compute the *Modified Expected Improvement* (MEI) at an arbitrary configuration $\mathbf{x}^{(*)}$ [33, 34]:

$$\begin{aligned} \text{MEI}(\mathbf{x}^{(*)}) = & (\widehat{Z}(\mathbf{x}_{\min}) - \widehat{Z}(\mathbf{x}^{(*)})) \Phi\left(\frac{\widehat{Z}(\mathbf{x}_{\min}) - \widehat{Z}(\mathbf{x}^{(*)})}{\widehat{s}(\mathbf{x}^{(*)})}\right) + \\ & \widehat{s}(\mathbf{x}^{(*)}) \phi\left(\frac{\widehat{Z}(\mathbf{x}_{\min}) - \widehat{Z}(\mathbf{x}^{(*)})}{\widehat{s}(\mathbf{x}^{(*)})}\right) \end{aligned} \quad (13)$$

where $\widehat{Z}(\mathbf{x}_{\min})$ is the stochastic kriging prediction at \mathbf{x}_{\min} (i.e. the point having the lowest sample mean for the scalarized objective among all feasible points already sampled), and $\phi(\cdot)$ and $\Phi(\cdot)$ are the standard normal density and standard normal distribution function. The notation $\widehat{s}(\mathbf{x}^{(*)})$ refers to the ordinary kriging standard deviation, which allows for balancing exploration and exploitation during optimization [13, 15, 41]:

$$\widehat{s}^2(\mathbf{x}^{(*)}) = k_{**} - k_* K_n^{-1} k_*^T \quad (14)$$

with $k_{**} = k(\mathbf{x}^{(*)}, \mathbf{x}^{(*)})$.

The acquisition function used in the proposed Bayesian optimization approach combines the probability of feasibility (predicted by the LR model) with the modified expected improvement. We refer to this acquisition function as *Constrained Modified Expected Improvement (CMEI)*:

$$\text{CMEI}(\mathbf{x}) = \text{MEI}(\mathbf{x}) * P(y = 1 | \mathbf{x}, \beta) \quad (15)$$

The optimization of the acquisition function in Bayesian optimization tends to be non-trivial, as the function is often non-linear, non-convex and multimodal [39]; in this work, we use a *Particle Swarm Optimization* (PSO) metaheuristic to find the infill point that maximizes CMEI. This (single) configuration is evaluated with the expensive objectives, and its information is used to update the parameters of both metamodels (the GP model and the LR model). The algorithm continues searching for new infill points, varying the weights $\boldsymbol{\lambda}$ (see Eq. 11) at each iteration in order to find solutions across the entire Pareto front, until the computational budget is depleted. Our proposed algorithm thus only performs $k + I$ expensive evaluations, with k the number of configurations in the initial design and I the number of iterations performed when the stopping criterion is met. Evolutionary algorithms, by contrast, require many more expensive evaluations, as they start with a population size P (commonly containing between 50 and 100 individuals [27]), which tends to remain equally large over the G consecutive generations (hence, yielding $P(1 + G)$ expensive evaluations).

5. Design of numerical experiments

To test the proposed optimization approach outside the lab environment, and benchmark its performance against four popular constrained EAs (NSGA-II, C-MOEA/D, C-TAEA, C-MOPSO), a Matlab process simulator

was provided by the Joining & Materials Lab¹. This simulator predicts a lap shear strength of the sample (MPa), failure mode (adhesive, substrate or cohesive failure), sample production (in euros) and visual quality outcome (OK or not OK) based on the process parameters discussed above, in a matter of seconds. It is *not* meant to be a perfect digital twin of the true process (such cheap digital twin does not exist), but rather a tool for the *relative* comparison of the performance of the five algorithms, under different conditions, at almost zero cost. Table 1 shows the range of each process parameter considered in the optimization problem.

Table 1: Range of the process settings (input variables) considered in the optimization

ID	Variable	Min	Max
v1	Pre-processing	Yes or No	
v2	Power setting (W)	300	500
v3	Torch speed (mm/s)	5	250
v4	Distance between the torch and the sample (cm)	0.2	2
v5	Number of passes	1	50
v6	Time between plasma treatment and glue application (min)	1	120

Table 2 summarizes the parameters of the optimization algorithms. The simulator allows the analyst to experiment with different levels of noise. In real life, multiple factors cause noise to occur. One of these is the so-called *contact angle*²: this typical measure reflects the extent to which the adhesive can maintain good contact with the material. This is important to achieve a strong adhesive bond. The contact angle depends on the type of material but also on impurities or contaminants such as wax, oil, plasticizers etc. present on the material surface. Even though all samples in our setting are made of the same material, variations in the degree of these contaminants occur across samples, implying variations in contact angle. These result in noisy measurements of the final break strength of the bonded joints. A realistic value for the *standard deviation of the contact angle* is $\gamma = 30\%$ of the mean, which is what we use in our experiments.

Given the experimental setting in Table 2, each algorithm evaluates exactly 60 process configurations in the expensive way, with 5 replications per configuration (i.e., 300 expensive evaluations in total). Our Bayesian optimization approach uses an initial design of 20 process configurations (note that this is smaller than the usual choice of $k = 10d$); exactly one infill point

¹<https://www.flandersmake.be>

²Other noise factors could not be controlled in the simulator, so they are not further discussed.

Table 2: Summary of the parameters of the optimization approaches

Setting	MO-GP	Evolutionary algorithms
Size of initial design/population		LHS: $N = 20$
Crossover probability	-	0.5 (C-MOEA/D); 0.9 o.w
Mutation probability	-	0.5
Reference directions	-	19 (C-TAEA); 3 (C-MOEA/D)
Inertia weight	-	0.4 (C-MOPSO)
C1 factor	-	2 (C-MOPSO)
C2 factor	-	2 (C-MOPSO)
Max velocity (%)	-	5 (C-MOPSO)
Replications		$r = 5$
Iterations	40	2
Acquisition function	CMEI	-
Acquisition function optimization	PSO *	-
Kernel	Gaussian	-

* The PSO algorithm was configured as follows: swarm size = 50, max iterations=1800, max stall iterations = 10, tolerance = $1e^{-6}$

is then added in each of the following 40 iterations. The EAs, by contrast, uses an initial population size of 20 process configurations; in each of the 2 successive generations, a novel population is constructed having the same size. As common in the literature, the fitness of the configuration outcomes is evaluated based on their sample means over the 5 replications (note that, by doing so, the EAs thus implicitly ignore the fact that this sample mean is in itself noisy and, hence, uncertain). The MO-GP approach takes into account both the sample mean and the sample variance though, as explained in Section 4. While a total budget of 300 evaluations may seem high, it allows us to also study the progress the algorithms would have obtained at lower budgets, as illustrated below.

We evaluate the quality of the resulting fronts using the hypervolume (HV) indicator [2], applied to the sample means. The hypervolume is the volume of the objective space that is dominated by the front obtained, w.r.t. a reference point. The larger the hypervolume, the better the quality of the front obtained. We use the algorithm proposed in [12] to compute this indicator. As the front obtained by the algorithms may depend on the initial design, we performed 50 macro-replications: each macro-replication starts with a different initial design, on which the algorithms then start their calculations.

6. Results

To gain some insight into the objective space to be explored by the algorithms under idealized conditions (i.e., if the contact angle could be perfectly controlled), Figure 6 shows the mean responses of the simulator on a set of 60 000 process configurations (with $\gamma = 0\%$; these configurations were determined through Halton sampling, and each configuration was replicated five times). Interestingly, the feasible solutions seem to be clustered in areas with high break strength; moreover, the use of pre-processing seems to merely lead to a cost increase, while the resulting gains in break strength are very scarce, and only minor. The Pareto optimal (feasible) points estimated by means of these Halton results, under these idealized conditions ($\gamma = 0\%$), serve as the benchmark Pareto front to judge the quality of the competing optimization algorithms.

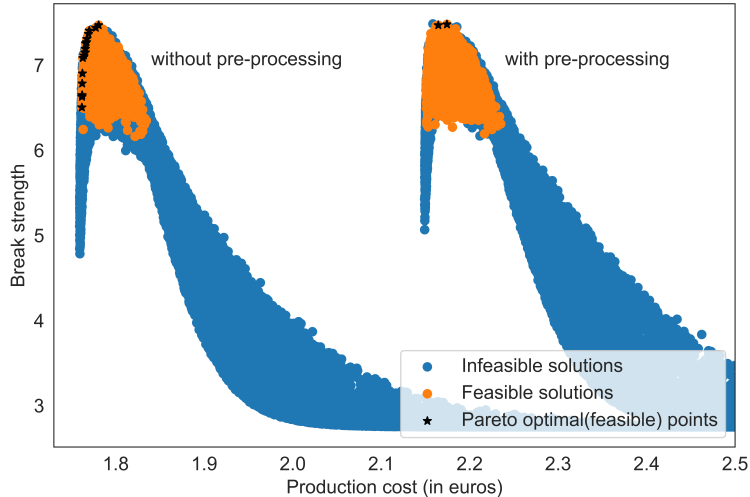


Figure 6: Sample mean of break strength versus production cost, estimated by the simulator for 60 000 random process configurations ($\gamma = 0\%$)

Figure 7 shows the final *best* Pareto front obtained by MO-GP over 50 macro-replications (along with the *median* and *worst* fronts), for $\gamma = 30\%$. Clearly, the best Pareto front obtained by MO-GP is very close to the ideal Pareto front estimated by means of the Halton set exploration. MO-GP also leads to a *faster* increase in HV, in terms of the number of expensive evaluations performed, than all other algorithms. This is evident from Figure 8, which shows the evolution of the *average* hypervolume obtained (across macro-replications) during the optimization process (again, for $\gamma = 30\%$). As mentioned before, all algorithms start from the same initial designs (consisting of 20 configurations). MO-GP thus is able to obtain better quality results for the Pareto front than the other algorithms, particularly at very limited budgets. This makes the algorithm better suited than the others in

settings with expensive evaluations. The plot also shows a dashed line, evaluating the hypervolume found by MO-GP under idealized conditions (i.e., $\gamma = 0\%$). As shown, the HV curve under realistic conditions ($\gamma = 30\%$) almost coincides with the one under ideal conditions, which illustrates that the presence of noise in realistic settings does not hurt the performance of MO-GP (as we expect; recall from Section 4 that the algorithm accounts for noise explicitly, both in the GPR model and in the infill criterion). This is also evident from Table 3, which shows the results for the average HV, along with those of the average modified Inverted Generational Distance (IGD+) [19]. This metric quantifies the distance between the Pareto front obtained by the algorithms and the ideal front obtained in the Halton experiment of Figure 6. As shown, MO-GP yields Pareto fronts that are on average closer to this ideal front.

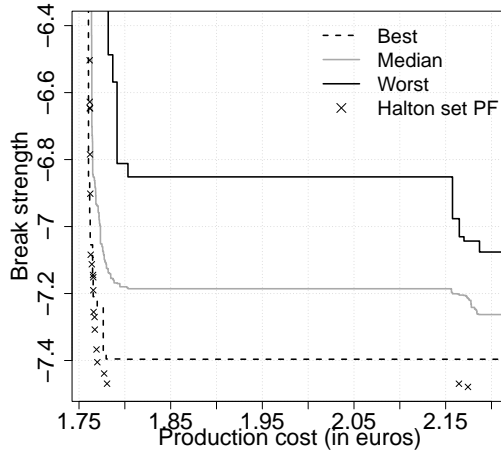


Figure 7: Best, median and worst Pareto front obtained for MO-GP when the noise is ($\gamma = 30\%$). The Y-axis is inverted to allow for minimization of both objectives

We observe a substantial difference in performance between MO-GP and the popular NSGA-II algorithm. Further analysis reveals that $\pm 77\%$ of the Pareto-optimal solutions put forward by NSGA-II use preprocessing (i.e., they are located in the bump at the right hand side of Figure 6), showing that the algorithm tends to "miss" solutions that do *not* require preprocessing (left hand bump in Figure 6). For MO-GP, $\pm 46\%$ of the solutions skip preprocessing; the algorithm is thus able to detect optimal solutions in both "bumps". Figure 9 analyzes the differences in the Pareto-optimal process configurations for the other input variables. Also here, the results show that the Bayesian algorithm succeeds in finding solutions that are better spread *across* the different ranges of all input variables, whereas NSGA-II clearly tends to focus on regions with higher values for plasma power and

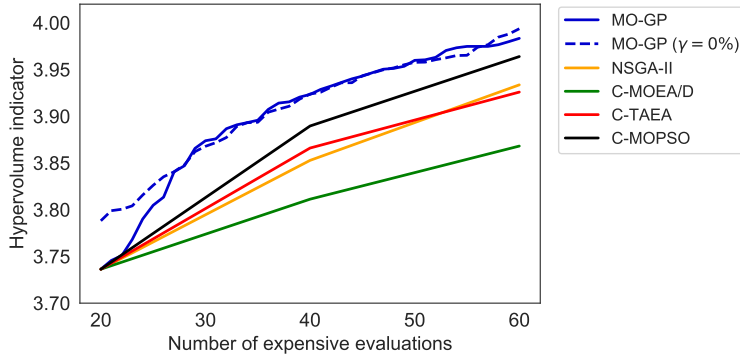


Figure 8: Evolution of the hypervolume (average of 50 macro-replications) of the Pareto-optimal solutions throughout the search, for $\gamma = 30\%$ (the calculations are based on the reference point with production cost=3, break strength=4). The dashed line evaluates the hypervolume of the Pareto-optimal points found by MO-GP when $\gamma = 0\%$

torch speed, and lower number of passes. Analogous figures comparing the MO-GP results with those of C-MOPSO, C-TAEA, and C-MOEA/D are shown in Appendix A. These algorithms detect solutions that are spread well across the different input ranges, yet, as evident from the HV results in Figure 8, the resulting Pareto fronts obtained have a lower average quality.

Table 3: Average IGD+ and HV of the fronts obtained over 50 macro-replications, for $\gamma = 30\%$. The best results are shown in bold

	IGD+	HV
MO-GP	0.1013	3.9834
C-MOPSO	0.1060	3.9639
C-TAEA	0.1217	3.9259
NSGA-II	0.1197	3.9336
C-MOEA/D	0.1513	3.8681

7. Conclusions

In this paper, we apply a constrained Bayesian optimization algorithm to solve a bi-objective problem related to the adhesive bonding process of materials (maximizing break strength while minimizing production costs). As experiments are expensive, the budget for evaluations is small. The proposed Bayesian approach is shown to clearly outperform competing evolutionary algorithms, which are commonly used in engineering design when solving general multi-objective, constrained problems. The difference lies in the way the experimental design is guided throughout the search: the Bayesian approach selects infill points based on an (explainable) acquisition function, which is related to the expected merit of the new infill point for the

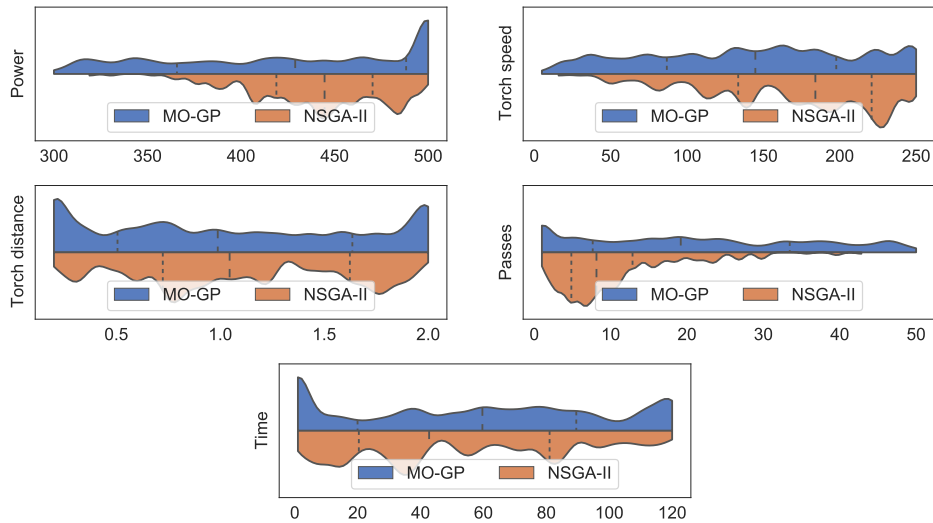


Figure 9: Probability distributions of the Pareto-optimal input values obtained by MO-GP and NSGA-II, across 50 macro-replications. The dashed lines represent the 25%, 50% (median), and 75% percentiles of the observed distributions.

optimization. The classification model embedded in the Bayesian approach ensures that the search focuses on infill points that have high probability of being feasible. Moreover, the GPR model used in the Bayesian approach accounts for the noise on the objectives, whereas the evolutionary algorithms rely on the (noisy) sample means as information to guide the search. In evolutionary approaches such as NSGA-II, by contrast, the search is guided by (black box, hard-to-tune) evolutionary operators. The success of such evolutionary process is largely dependent on the availability of sufficient experimentation budget, which is not always the case in practice.

We are convinced that the use of Bayesian approaches holds great promise in solving noisy and expensive engineering problems, in terms of both search efficiency (i.e., finding solutions within limited budget) and search effectiveness (i.e., yielding high-quality solutions). Future research will focus on the development of an interactive software tool, allowing lab experts to validate the results generated by the algorithm in a real-life test environment, and to apply this type of algorithm also to other process optimization problems.

Acknowledgments

This work was supported by the Flanders Artificial Intelligence Research Program (FLAIR), the Research Foundation Flanders (FWO Grant 1216021N), and Flanders Make vzw.

References

- [1] Ankenman, B., Nelson, B.L., Staum, J., 2010. Stochastic kriging for simulation metamodeling. *Operations Research* 58, 371–382. doi:<https://doi.org/10.1109/WSC.2008.4736089>.
- [2] Auger, A., Bader, J., Brockhoff, D., Zitzler, E., 2012. Hypervolume-based multiobjective optimization: Theoretical foundations and practical implications. *Theoretical Computer Science* 425, 75–103. doi:<https://doi.org/10.1016/j.tcs.2011.03.012>.
- [3] Brockmann, W., Geiß, P.L., Klingen, J., Schröder, K.B., 2008. Adhesive bonding: materials, applications and technology. John Wiley and Sons.
- [4] Brownlee, A.E., Wright, J.A., 2015. Constrained, mixed-integer and multi-objective optimisation of building designs by nsga-ii with fitness approximation. *Applied Soft Computing* 33, 114–126. <https://doi.org/10.1016/j.asoc.2015.04.010>.
- [5] Budhe, S., Banea, M., De Barros, S., Da Silva, L., 2017. An updated review of adhesively bonded joints in composite materials. *International Journal of Adhesion and Adhesives* 72, 30–42.
- [6] Cavezza, F., Boehm, M., Terryn, H., Hauffman, T., 2020. A review on adhesively bonded aluminium joints in the automotive industry. *Metals* 10. <https://doi.org/10.3390/met10060730>.
- [7] Chiarello, F., Belingheri, P., Fantoni, G., 2021. Data science for engineering design: State of the art and future directions. *Computers in Industry* 129, 103447. <https://doi.org/10.1016/j.compind.2021.103447>.
- [8] Chugh, T., Sindhya, K., Hakanen, J., Miettinen, K., 2017. A survey on handling computationally expensive multiobjective optimization problems with evolutionary algorithms. *Soft Computing* , 1–30<https://doi.org/10.1007/s00500-017-2965-0>.
- [9] Corbett, M., Sharos, P.A., Hardiman, M., McCarthy, C.T., 2017. Numerical design and multi-objective optimisation of novel adhesively bonded joints employing interlocking surface morphology. *International Journal of Adhesion and Adhesives* 78, 111–120. <https://doi.org/10.1016/j.ijadhadh.2017.06.002>.
- [10] Correia, S., Anes, V., Reis, L., 2018. Effect of surface treatment on adhesively bonded aluminium-aluminium joints regarding aeronautical structures. *Engineering Failure Analysis* 84, 34–45. <https://doi.org/10.1016/j.engfailanal.2017.10.010>.

- [11] Deb, K., Pratap, A., Agarwal, S., Meyarivan, T., 2002. A fast and elitist multiobjective genetic algorithm: Nsga-ii. *IEEE transactions on evolutionary computation* 6, 182–197. doi:<https://doi.org/10.1109/4235.996017>.
- [12] Fonseca, C.M., Paquete, L., López-Ibáñez, M., 2006. An improved dimension-sweep algorithm for the hypervolume indicator, in: 2006 IEEE international conference on evolutionary computation, IEEE. pp. 1157–1163. <https://doi.org/10.1109/CEC.2006.1688440>.
- [13] Forrester, A., Sobester, A., Keane, A., 2008. *Engineering Design via Surrogate Modelling (A Practical Guide)*. 1st ed., John Wiley and Sons, West Sussex, UK.
- [14] Gao, Y.L., Qu, M., 2012. Constrained multi-objective particle swarm optimization algorithm, in: *International Conference on Intelligent Computing*, Springer. pp. 47–55.
- [15] Gramacy, R.B., 2020. *Surrogates: Gaussian process modeling, design, and optimization for the applied sciences*. Chapman and Hall/CRC.
- [16] Habenicht, G., 2008. *Applied adhesive bonding: a practical guide for flawless results*. John Wiley and Sons.
- [17] Horn, D., Dagge, M., Sun, X., Bischl, B., 2017. First investigations on noisy model-based multi-objective optimization, in: *International Conference on Evolutionary Multi-Criterion Optimization*, Springer. pp. 298–313. doi:https://doi.org/10.1007/978-3-319-54157-0_21.
- [18] Hunter, S.R., Applegate, E.A., Arora, V., Chong, B., Cooper, K., Rincón-Guevara, O., Vivas-Valencia, C., 2019. An introduction to multiobjective simulation optimization. *ACM Trans. Model. Comput. Simul.* 29, 7:1–7:36. doi:<http://doi.acm.org/10.1145/3299872>.
- [19] Ishibuchi, H., Masuda, H., Tanigaki, Y., Nojima, Y., 2015. Modified distance calculation in generational distance and inverted generational distance, in: *International conference on evolutionary multi-criterion optimization*, Springer. pp. 110–125. https://doi.org/10.1007/978-3-319-15892-1_8.
- [20] Jain, H., Deb, K., 2013. An evolutionary many-objective optimization algorithm using reference-point based nondominated sorting approach, part ii: Handling constraints and extending to an adaptive approach. *IEEE Transactions on evolutionary computation* 18, 602–622.
- [21] Jones, D.R., Schonlau, M., Welch, W.J., 1998. Efficient global optimization of expensive black-box functions. *Journal of Global optimization* 13, 455–492. <https://doi.org/10.1023/A:1008306431147>.

- [22] Knowles, J., 2006. Parego: A hybrid algorithm with on-line landscape approximation for expensive multiobjective optimization problems. *IEEE Transactions on Evolutionary Computation* 10, 50–66. <https://doi.org/10.1109/TEVC.2005.851274>.
- [23] Labbé, S., Drouet, J.M., 2012. A multi-objective optimization procedure for bonded tubular-lap joints subjected to axial loading. *International journal of adhesion and adhesives* 33, 26–35. <https://doi.org/10.1016/j.ijadhadh.2011.09.005>.
- [24] Li, K., Chen, R., Fu, G., Yao, X., 2018. Two-archive evolutionary algorithm for constrained multiobjective optimization. *IEEE Transactions on Evolutionary Computation* 23, 303–315.
- [25] Li, M., Li, G., Azarm, S., 2008. A kriging metamodel assisted multi-objective genetic algorithm for design optimization. *Journal of Mechanical Design* 130. <https://doi.org/10.1115/1.2829879>.
- [26] Licari, J.J., Swanson, D.W., 2011. Adhesives technology for electronic applications: materials, processing, reliability. William Andrew.
- [27] Lobo, F.G., Lima, C.F., 2005. A review of adaptive population sizing schemes in genetic algorithms, in: *Proceedings of the 7th annual workshop on Genetic and evolutionary computation*, pp. 228–234.
- [28] Loeppky, J., Sacks, J., Welch, W., 2009. Choosing the sample size of a computer experiment: a practical guide. *Technometrics* 51, 366–376.
- [29] Marler, R.T., Arora, J.S., 2004. Survey of multi-objective optimization methods for engineering. *Structural and Multidisciplinary Optimization* 26, 369–395. doi:<https://doi.org/10.1007/s00158-003-0368-6>.
- [30] Miettinen, K., 1999. *Nonlinear multiobjective optimization*. volume 12. Springer Science & Business Media.
- [31] Miettinen, K., Mäkelä, M.M., 2002. On scalarizing functions in multi-objective optimization. *OR spectrum* 24, 193–213. doi:<https://doi.org/10.1007/s00291-001-0092-9>.
- [32] Pocius, A., 2021. *Adhesion and adhesives technology: an introduction*. Carl Hanser Verlag GmbH Co KG.
- [33] Quan, N., Yin, J., Ng, S.H., Lee, L.H., 2013. Simulation optimization via kriging: a sequential search using expected improvement with computing budget constraints. *Iie Transactions* 45, 763–780. doi:<https://doi.org/10.1080/0740817X.2012.706377>.

- [34] Rojas-Gonzalez, S., Jalali, H., Nieuwenhuyse, I.V., 2020. A multiobjective stochastic simulation optimization algorithm. *European Journal of Operational Research* 284, 212–226. doi:<https://doi.org/10.1016/j.ejor.2019.12.014>.
- [35] Rojas-Gonzalez, S., van Nieuwenhuyse, I., 2020. A survey on kriging-based infill algorithms for multiobjective simulation optimization. *Computers and Operations Research* 116, 104869. doi:<https://doi.org/10.1016/j.cor.2019.104869>.
- [36] da Silva, L., Ochsner, A., Adams, R., Spelt, J., 2011. *Handbook of adhesion technology*. Springer Science & Business Media.
- [37] Tao, T., Zhao, G., Ren, S., 2020. An efficient kriging-based constrained optimization algorithm by global and local sampling in feasible region. *Journal of Mechanical Design* 142.
- [38] Williams, C.K., Rasmussen, C.E., 2006. *Gaussian processes for machine learning*. volume 2. MIT press Cambridge, MA.
- [39] Wilson, J., Hutter, F., Deisenroth, M., 2018. Maximizing acquisition functions for bayesian optimization, in: Bengio, S., Wallach, H., Larochelle, H., Grauman, K., Cesa-Bianchi, N., Garnett, R. (Eds.), *Advances in Neural Information Processing Systems*, Curran Associates, Inc. URL: <https://proceedings.neurips.cc/paper/2018/file/498f2c21688f6451d9f5fd09d53edda7-Paper.pdf>.
- [40] Witten, I.H., Frank, E., Hall, M.A., 2011. *Data mining: practical machine learning tools and techniques*. 3 ed., Morgan Kaufmann.
- [41] Zhan, D., Xing, H., 2020. Expected improvement for expensive optimization: a review. *Journal of Global Optimization* 78, 507–544. doi:<https://doi.org/10.1007/s10898-020-00923-x>.
- [42] Zhou, A., Qu, B.Y., Li, H., Zhao, S.Z., Suganthan, P.N., Zhang, Q., 2011. Multiobjective evolutionary algorithms: A survey of the state of the art. *Swarm and Evolutionary Computation* 1, 32–49. doi:<https://doi.org/10.1016/j.swevo.2011.03.001>.

Appendix A. Input space analysis

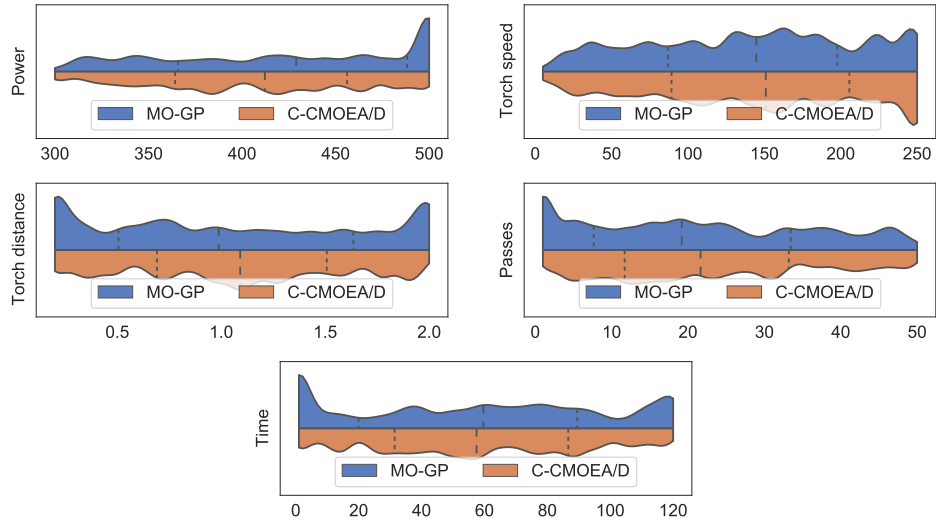


Figure A.1: Probability distributions of the Pareto-optimal input values obtained by MO-GP and C-MOEA/D, across 50 macro-replications. The dashed lines represent the 25%, 50% (median), and 75% percentiles of the observed distributions

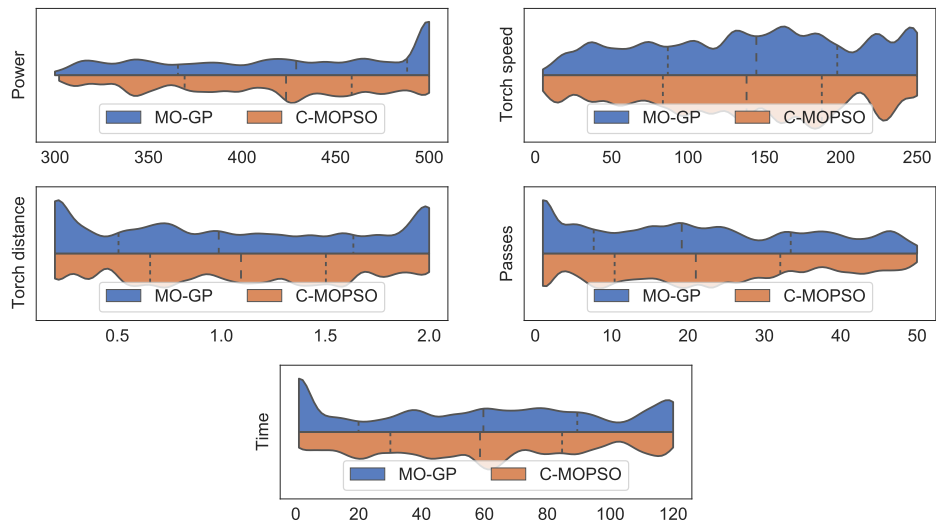


Figure A.2: Probability distributions of the Pareto-optimal input values obtained by MO-GP and C-MOPSO, across 50 macro-replications. The dashed lines represent the 25%, 50% (median), and 75% percentiles of the observed distributions

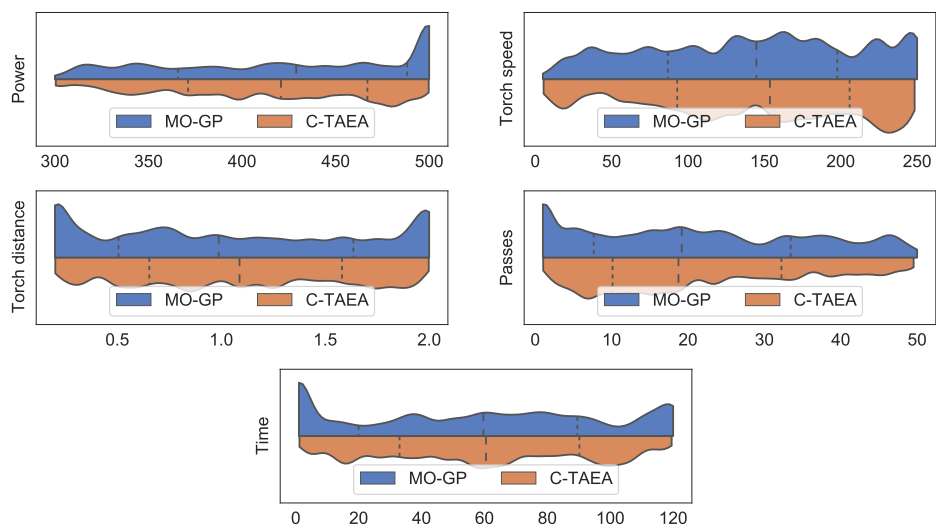


Figure A.3: Probability distributions of the Pareto-optimal input values obtained by MO-GP and C-TAEA, across 50 macro-replications. The dashed lines represent the 25%, 50% (median), and 75% percentiles of the observed distributions